

Chapter 2

ACCELERATOR AUGMENTATION

2.1 High current injector

Sugam Kumar, R. V. Hariwal, Kedar Mal, P. S. Lakshmi, Sarvesh Kumar, Rajeev Ahuja, V. V. V. Satyanarayana, Parmanand Singh, Yaduvansh Mathur, S. Venkataramanan, Chandra Pal, Ashok Kothari, P. Barua, Ruby Shanthi, Deepak K. Munda, Kundan Singh, R. K. Gurjar, Mukesh Kumar, G. O. Rodrigues, C. P. Safvan and Rajeev Mehta

This academic year witnessed a notable milestone in the High Current Injector (HCI) project with the acceleration of the HCI beam by the Superconducting Linac. The outcome of the test was partially successful with a Ne^{7+} beam accelerated through the initial 12 QWRs (quarter wave resonators) of the Linac. Due to a significantly large energy spread in the beam, which resulted in a large temporal spread, further acceleration was deemed unfeasible. Currently efforts are focused on identifying the underlying causes for this large energy spread. To reduce it, we are planning to operate Achromat-4 in energy dispersion mode and utilize a slit at its image plane to allow beam of the acceptable energy spread. Plans are also underway to conduct beam tests with higher A/q values, showcasing the facility's adaptability and to expand its operational capabilities. Fig. 2.1 shows the HCI facility.



Figure 2.1: High current injector facility.

2.1.1 ECR ion source

2.1.1.1 Performance of 18 GHz HTS ECR ion source and maintenance activities

The last academic year saw the operation of the source with oxygen beams for stability tests and neon beams for bunching tests, along with beam tests of the newly installed HEBT section of HCI up to the zero-degree beamline (that goes to the Superconducting Linac), all at an energy of 1.8 MeV/u. While minor maintenance tasks were swiftly handled, we encountered several significant maintenance challenges. These

2. ACCELERATOR AUGMENTATION

included cleaning of the ion source, resolving vacuum issues post-maintenance, addressing the failure of the extraction side cryocooler, cleaning of the GP tube column, and managing the failure of the Klystron

1. **Maintenance of ion source:** The ion source cavity had not been cleaned since the installation of the source in beam hall-3. The system was shut down for scheduled maintenance following the August beam acceleration test. Fig. 2.2(a) shows the dismantled parts of the ion source. After cleaning the ion source cavity and sandblasting the insulators, the Einzel assembly, injection side pumps, and ion source parts were reinstalled in reverse order, as shown in Fig. 2.2(b). Two blank-offs were fabricated for separate leak-testing of the ion source and Einzel assembly.

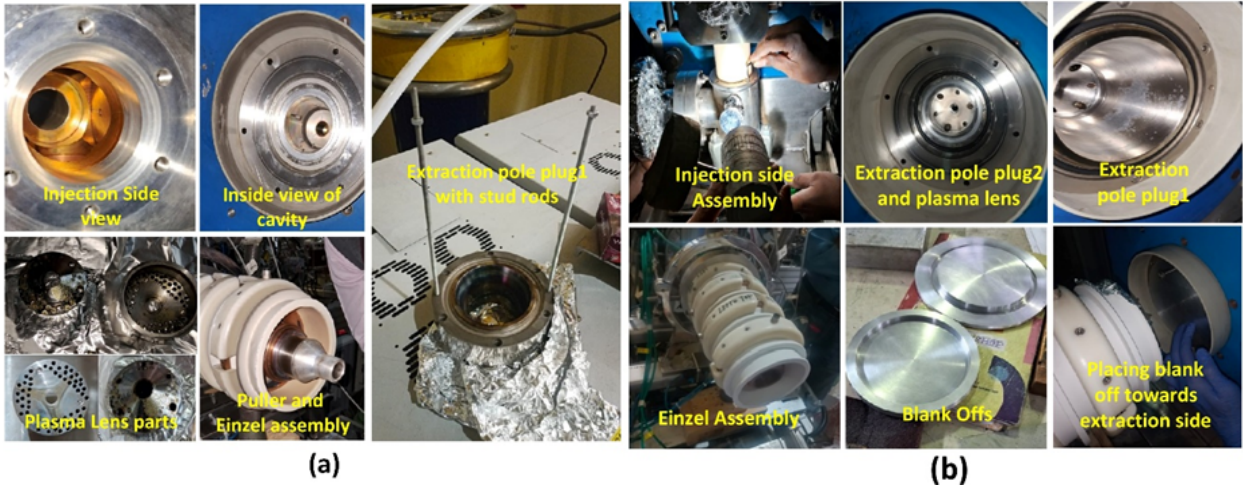


Figure 2.2: (a) View of the ion source parts before cleaning, (b) View of reinstalled parts of the ion source after cleaning.

During leak testing, a vacuum leak was found towards the extraction side of the source. However, the exact location of the leak could not be pinpointed due to numerous joints and O-rings. To prepare the ion source for the upcoming beam acceleration test, it was closed with a leak rate of 5×10^{-7} mbar l/s with full helium spray and achieved as low as 10^{-9} mbar l/s without helium spray. Fig. 2.3 illustrates the vacuum status of the ion source after maintenance for nearly 4 days, with both injection and extraction pressures fluctuating between 10^{-7} to 10^{-4} Torr.

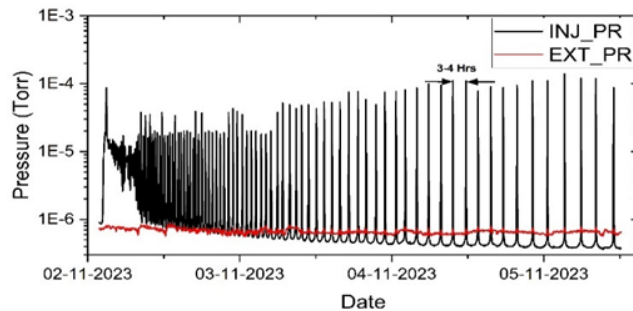


Figure 2.3: Vacuum fluctuations of ion source.

After inspecting the source drawings, both the injection and extraction sides of the ion source were reopened to replace the O-rings, as pole plug-2 had not been removed during the initial cleaning of the ion source cavity. The O-rings, specially the DC bias adaptor and pole plug-2, were found flattened, which were subsequently replaced with new ones. Following the replacement, no leaks were observed, and the ultimate leak rate improved to 3×10^{-9} mbar l/s with full helium spray. As depicted in Fig. 2.4, which illustrates the vacuum history of the ion source over nearly 3 days, the vacuum fluctuation issues were completely resolved.

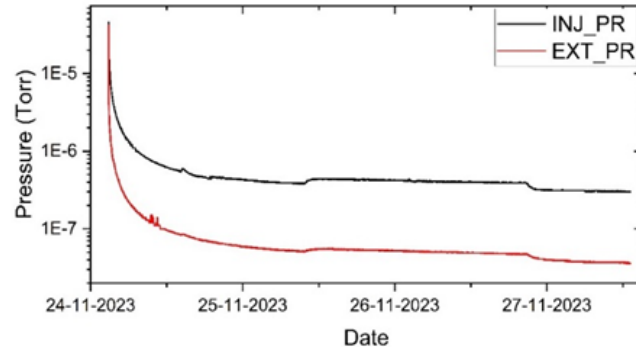


Figure 2.4: Vacuum of ion source without any fluctuations after replacements of O-rings

2. **Failure of extraction side cryocooler:** After completing the maintenance of the ion source, we observed a deterioration in the vacuum of cryostat 2 (CS2). While tracing the issue, the extraction side cryocooler (CC2) was found in stopped condition displaying a ‘Stall Warning’ as shown in Fig. 2.5(a).

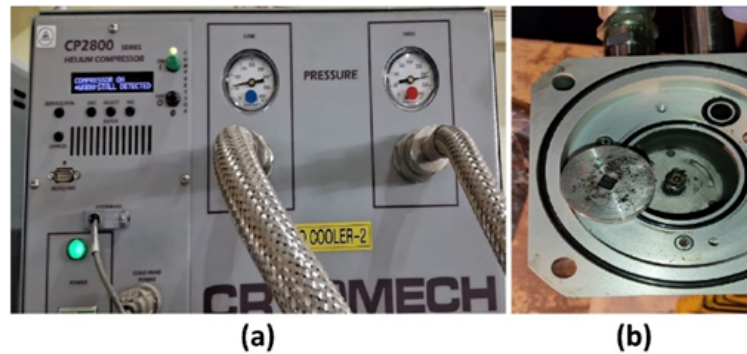


Figure 2.5: (a) CC2 display showing Stall Warning, (b) Damaged cold head motor of CS2.

Both cryocoolers (CC1 and CC2) have been in continuous operation since the installation of the ion source in beam hall-3. While diagnosing the issue, the cold head motor of cryostat 2 was found damaged as shown in Fig. 2.5(b). The damaged motor was subsequently removed and replaced with a spare motor. CC2 was recharged using Helium gas of purity 99.9999% to the recommended value of static pressure of 220 PSI using a vacuum manifold connected. Subsequently, the operation of the extraction side cryocooler was restored.

3. **Failure of Klystron:** Following the December beam acceleration test, a setback occurred when the Klystron failed to operate. Remarkably, the Klystron had been running continuously without any major breakdowns for the past few years. Upon diagnosing the issue, it was discovered that a Servo Stabilizer had gone bad. In Fig. 2.6, the Klystron can be seen alongside the faulty Servo Stabilizer. This unexpected failure prompted immediate attention to rectify the issue to ensure the smooth operation of the accelerator system
4. **Cleaning of GP tube column:** During the facility breakdown, we noticed deterioration in the GP tube column, particularly towards the resistor chain, although the inner section was clean. This deterioration likely occurred due to the improper arrangement of the resistor chain. To ensure stable voltages, the GP tube column was removed for sandblasting. Fig. 2.7(a) shows the sandblasting process of the deteriorated GP tube column.

Prior to cleaning, the resistance per gap was less than 2 G Ω , but after sandblasting it increased to approximately 100 G Ω at 10kV. Fig. 2.7(b) shows the resistance measurement using a Megger.

2. ACCELERATOR AUGMENTATION



Figure 2.6: Klystron along with the repaired Servo stabilizer.



Figure 2.7: (a) sandblasting and (b) resistance measurement of GP tube column using a Megger.

2.1.1.2 Beam stability test

In the previous year, the beam stability data was recorded using an O^{6+} beam for more than 8 hours at various beam parameters and system conditions as described in Table 2.1. The fluctuations in the beam intensity for all cases were only 100 nA at an input beam current of 7 μA . The stability of the beam, having an energy of 180 keV/u at the RFQ exit, can be seen in Fig. 2.8 when the input beam current was 6 μA .

2.1.1.3 Study of beam transmission through LEBT

The beam transmission through low energy beam transport (LEBT) section was studied using O^{6+} beam at various input beam energies with the deck OFF. To measure the transmission through the LEBT, the beam intensity was recorded at two Faraday cups: just after the analyser dipole magnet (FC_0-1) and just after the MHB (FC_02-1).

The beam intensities at both cups and the transmission through the LEBT at various input energies are shown in Fig. 2.9. The maximum transmission was found to be approximately 40% through the LEBT at

Table 2.1: The various beam parameters and system conditions for beam stability tests.

Beam	Energy	Extractor	Deck	MHB	RFQ
DC	6 keV/u	16.33 kV	OFF	OFF	OFF
DC	8 keV/u	21.33 kV	OFF	OFF	OFF
DC	8 keV/u	16.33 kV	5 kV	OFF	OFF
Pulse	8 keV/u	16.33 kV	5 kV	ON	OFF
Pulse	180 keV/u	16.33 kV	5 kV	ON	ON

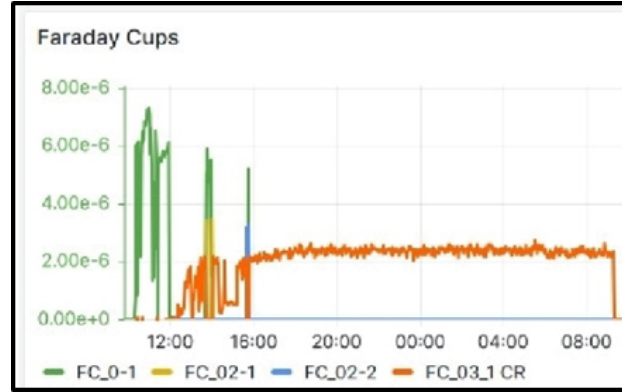


Figure 2.8: Beam stability of O^{6+} at the exit of RFQ over a period of 16 hours.

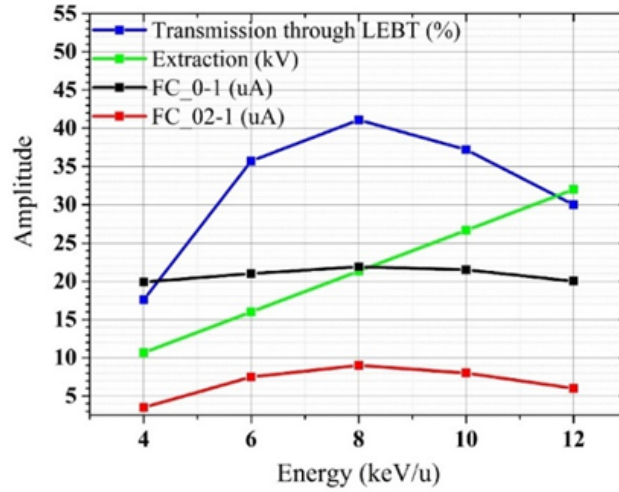


Figure 2.9: Variation of beam intensities and transmission through LEBT as a function of input energy.

an input energy of 8 keV/u, and with optimized parameters of the LEBT it could not be maximized beyond 60%. To determine the cause of beam loss, the LEBT section was opened from the location of the GP tube column during the breakdown of the facility. It was found that the beam was cutting at two places: at the 25 mm aperture of the Faraday cup (FC_0-2, just before the MHB) and at the MHB grids.

2.1.2 Multi-harmonic buncher

The Multi Harmonic Buncher (MHB) system has been designed to deliver bunched beams to the RFQ whenever necessary. In August 2023, Ne^{7+} beam was successfully extracted, bunched, and accelerated through all the cavities to reach the target energy of 1.8 MeV/u. This was achieved with a current of 350 nA and a bunch width of 24 ns, all without using Spiral Buncher 2 and 3.

In December 2023, further progress was made as the same Ne^{7+} beam was tuned, resulting in the acceleration of the 36 MeV beam through the first 12 cavities of the Linac to an energy of 77.1 MeV (41.1 MeV gain from Linac), albeit with a low current of few nA. Beam could not be accelerated further due to reasons as described in section 2.1.6.5 below. Throughout these tests the MHB system underwent numerous tuning iterations to enhance beam transmission through the RF cavities. Challenges arose with the pickup problem observed in the Fast Faraday Cup (FFC), primarily traced back to the high voltage suppressor power supply. Efforts are underway to mitigate this issue by enclosing the suppressor power supply within a Faraday Cage, reducing pickup signals significantly. Additionally, plans include replacing RF cables with 100% shielded high-quality ones and minimizing RF connectors to improve signal integrity. During testing of HCI beam with the Superconducting Linac, synchronization with a common clock was employed, necessitating slight adjustments in the MHB electronics controller to ensure seamless beam delivery from HCI to the Linac.

2. ACCELERATOR AUGMENTATION

2.1.3 Radio-frequency quadrupole

In RFQ, one of the key challenges encountered was the burning of the RF contacts on the frequency tuning plates within the RFQ cavity, occurring at high power levels of around 40 kW.

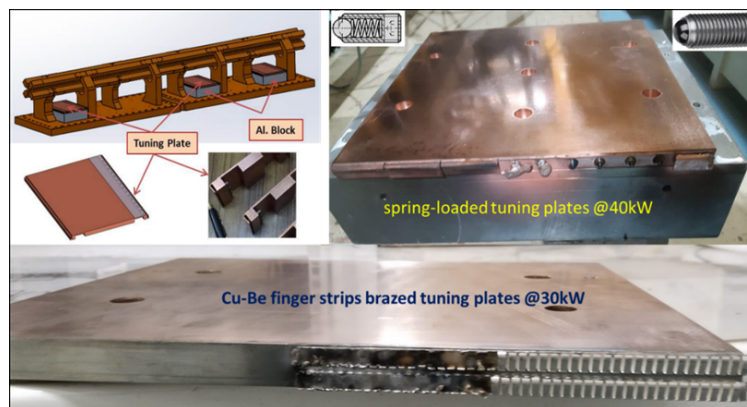


Figure 2.10: Photographs of burnt RF contacts of the RFQ frequency tuning plates.

This limitation hindered the conditioning of the cavity at the full power of 90 kW required for accelerating a beam of $A/q=6$. To address this issue, various solutions were explored, including the soldering of double Be-Cu finger strips as shown in Fig. 2.10, but it did not prove successful beyond 30 kW. In response to the excessive heat generated across the RF contacts, a decision was made to manufacture water-cooled tuning plates with direct water cooling of the entire RF contact line. A water-cooled tuning plate was machined and installed in the RFQ section as shown in Fig. 2.11. This solution aimed to effectively extract the excess heat and prevent the burning of the RF contacts. The implementation of water-cooled tuning plates is a significant step toward overcoming the issue of RF contact. Presently, the conditioning process of the cavity with the new tuning plate is going on. The machining of two more tuning plates is under process.

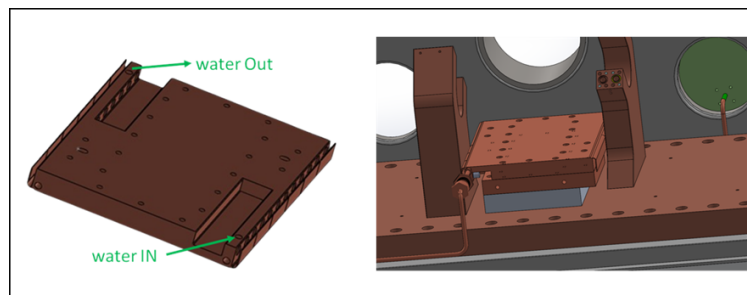


Figure 2.11: Schematic of the water-cooled frequency tuning of the RFQ.

2.1.4 Spiral buncher

Last year, the fabrication of Spiral Bunchers no. 2 and 3 was completed. To ensure their optimal performance, low-power RF measurements were conducted to verify the cavities' resonance frequency and quality factor. Following this, Spiral Bunchers 2 and 3 were installed in beam halls 3 and 1, respectively, positioned after achromats 1 and 3, as shown in Fig. 2.12. Currently, we are performing the RF power conditioning of these cavities.

2.1.5 Drift tube linac

During the operation of the DTL cavities, two major issues were encountered, prompting necessary maintenance.



Figure 2.12: Photographs of installation of Spiral Buncher 2 and 3 in BH-3 and 1, respectively.

2.1.5.1 Water leakage from push-fit PU tubes

A major issue arose due to a water leakage caused by the push-fit type PU tubes connected to the RF power couplers. These tubes got opened during operation, resulting in the sprinkling of water within BH-3 area. This affected the vacuum display units of the DTLs as well as other critical components like RF amplifiers and magnet power supplies. To address the problem, the push-fit arrangement of the outer cooling channels was replaced with Ferrule connectors, providing a more secure and reliable connection, although the push-fit connector of the inner conductor could not be replaced due to design constraints. The cooling channels to the outer and inner conductors are shown in Fig. 2.13.

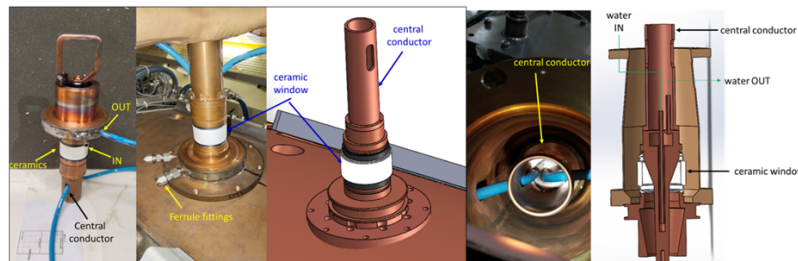


Figure 2.13: Photographs and schematics of the push-fit PU tubes for cooling the RF power coupler.

2.1.5.2 Stuck frequency tuning rod in DTL-4

Another issue encountered was the frequency tuning rod in DTL-4 that got stuck during operation. Upon inspection, it was found that the Be-Cu finger strips, initially placed for mechanical stability, were stuck to the copper wall (Fig. 2.14). To prevent the occurrence of such problems in future, it was decided to remove all Be-Cu finger strips from all the six DTL cavities. To ensure that removing these strips did not affect the resonant frequency and quality factor of the cavities, low-power RF parameters were measured which were found to be unaffected.

2.1.6 Beamline installation up to linac

For coupling the HCI beamline to the SC Linac, the HEBT section had to be first completed, which was undertaken in four stages as described below:

2.1.6.1 Installation up to achromat-2

The primary objective in this phase was to install all available beamline components followed by beam acceleration. Due to the non-availability of all the components we could only complete the installation up to Achromat-2. The N^{6+} beam of 1.8 MeV/amu having mass-to-charge ratio (A/q) of 2.33 was transported to

2. ACCELERATOR AUGMENTATION

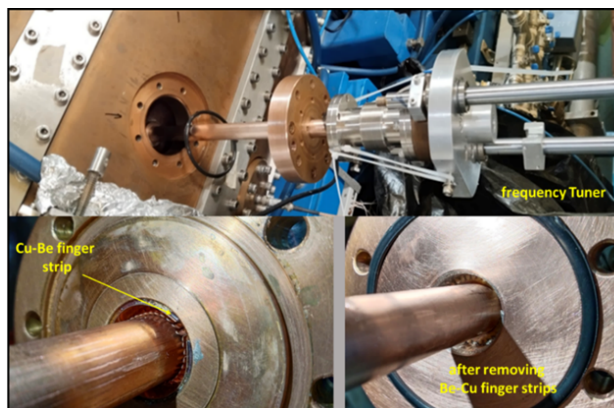


Figure 2.14: Photographs of the frequency tuner before and after removal of the Cu-Be finger strips.

Achromat-2. Analysed current of 280 nA was measured at the Faraday Cup FC-06-1 located immediately after the achromat, as shown in Fig. 2.15.

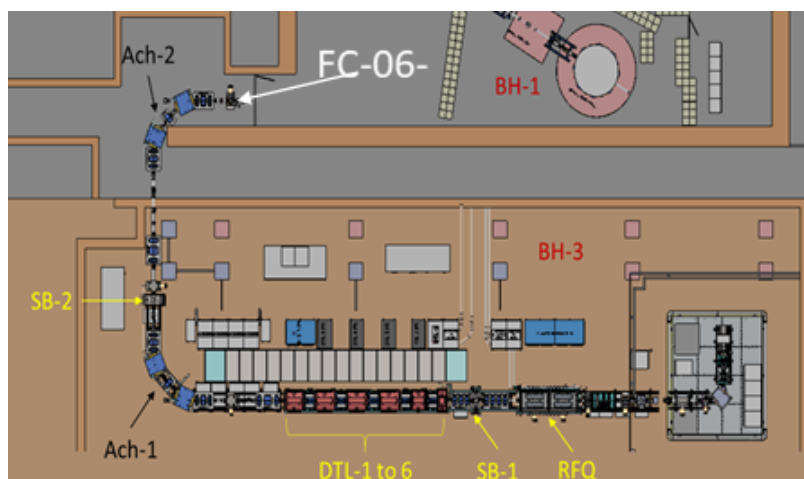


Figure 2.15: Layout of beamline installation up to Achromat 2.

2.1.6.2 Installation of complete HEBT section up to zero-degree beam line

During this phase, installation of the complete HEBT section was done. To check the functionality of all the installed beamline components up to the Zero-degree Beam Line (that goes to the SC Linac), as shown in Fig. 2.16, O^{6+} ion beam with a mass-to-charge ratio (A/q) of 2.66 was used. The beam was accelerated through the RFQ only, as the aim was to check the functionalities of all the installed components, power supplies and installed utilities. The beam was transported through the HEBT section and was analysed at the Faraday Cup FC-08-1. This test enabled us to troubleshoot and address the issues encountered. No major problem was faced except the malfunctioning of a couple of Faraday Cups (FC-05-1 and FC-07-1) and problems with the Magnetic Steerer (MS06). These issues were promptly resolved, ensuring the full functioning of the HEBT section.

2.1.6.3 Beam acceleration up to zero-degree beam line

During this test we aimed to transport 1.8 MeV/u beam up to the zero-degree beamline. The Ne^{7+} ion beam of mass-to-charge ratio (A/q) of 2.85 was used for this purpose. The beam was analysed at the Faraday Cup FC-08-1 located in the zero degree beam line, just before the Superbuncher of the SC-Linac. The measured current was 130 nA.

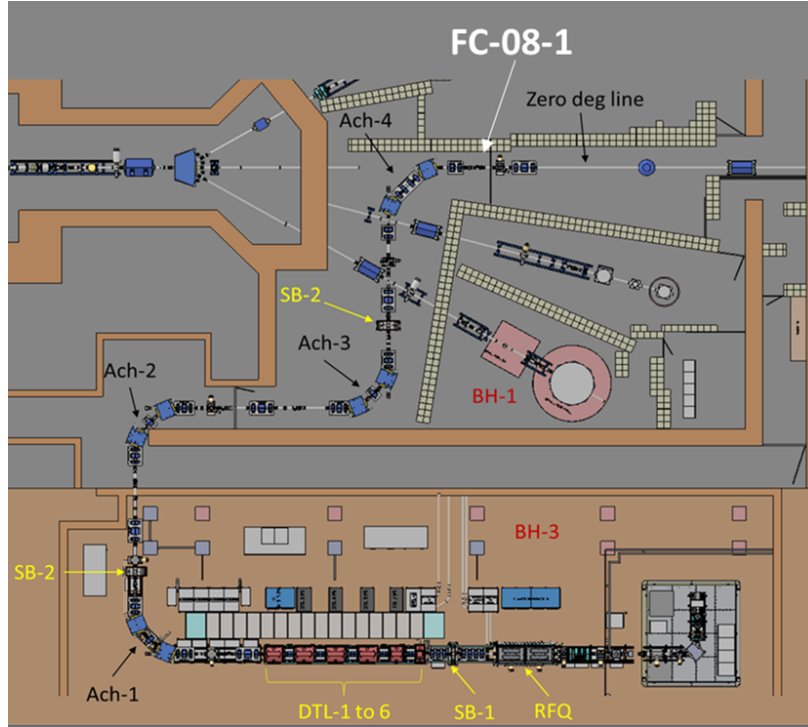


Figure 2.16: Layout of the completer beamline installation up to zero-degree beam line.

Table 2.2: Energy gain through SC-linac cavities.

SC-linac cavity	Energy gain (MeV)	Final beam energy (MeV)
QWR R11	2.26	38.26
QWR R12	3.01	41.27
QWR R13	3.25	44.52
QWR R14	3.37	47.89
QWR R15	2.73	50.62
QWR R16	4.81	55.43
QWR R17	2.96	58.39
QWR R18	3.86	62.25
QWR R21	3.05	65.3
QWR R22	3.65	68.95
QWR R23	4.37	73.32
QWR R24	3.78	77.10

2.1.6.4 Beam acceleration tests through SC-linac cavities

The Ne^{7+} beam from the ECR ion source was accelerated through the HCI before injecting it into the SC-Linac. This involved injecting the bunched beam from the Multi Harmonic Buncher (MHB) into the Radio Frequency Quadrupole (RFQ) followed by the Drift Tube Linac section to achieve the required energy gain of 1.8 MeV/u. To understand the characteristics of the beam, its energy and time width were measured using a Surface Barrier Detector (SBD) located at the entrance of the SC Linac. The measured beam energy was 36 MeV having a time width of 24 ns (FWHM) without using Spiral Buncher-2 and 3. With the use of the HEBT-Spiral Buncher-3 the time spread of the bunch was reduced to 1.08 ns, having a total energy spread of 1.3% of the beam energy (468 keV FWHM). This was measured and confirmed using the SBD.

2.1.6.5 Beam acceleration through SC-linac QWRs

By optimizing the Superbuncher field, the best time-width of 854 ps FWHM was achieved at the entrance of the Linac for further acceleration by the quarter wave resonators (QWR). The beam could be accelerated through the first 12 QWRs. The beam energy and energy gain after each QWR are listed in Table 2.2.

2. ACCELERATOR AUGMENTATION

2.1.6.6 Issues due to energy spread

Despite progress, challenges were faced related to the energy spread of the beam. After accelerating the beam through QWR R18, an increase in energy spread was observed, as shown in Fig. 2.17(a). Subsequent cavities witnessed a continued increase in the energy spread, with QWR R21 marking a critical point where the spread overshadowed the main peak, as shown in Fig. 2.17(b). Beyond QWR R24, identifying the main peak became unfeasible, halting further acceleration process.

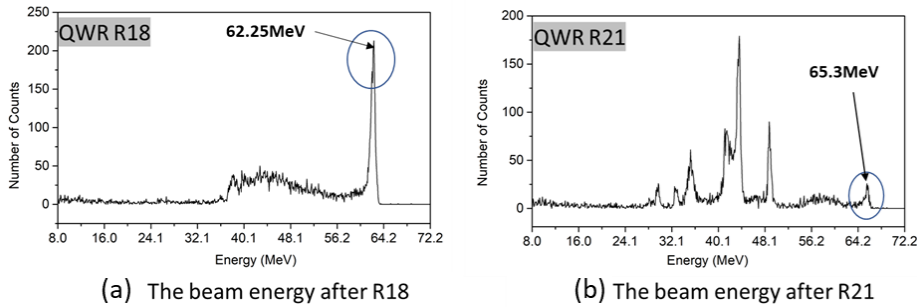


Figure 2.17: The accelerated beam energy after SC-Linac cavities R18 and R21.

In conclusion, despite encountering challenges with energy spread, our achievements in accelerating the Ne^{7+} beam of 36 MeV with an energy spread of 1.3% (468 keV FWHM) and optimizing the time width from 24 ns to 1.08 ns using SB-3, are promising. However, the significant energy spread remains a hurdle for further acceleration, prompting focused efforts to identify its root causes. To address this issue, we plan to operate Achromat-4 in energy dispersion mode and use a slit at the image plane of this achromat to allow beam of the acceptable energy spread, though this may cause some reduction in the beam current. Furthermore, we are intensifying our efforts to conduct beam tests with the design $A/Q=6$, aiming to advance towards the commissioning of the High Current Injector. We are also addressing the issue with the MHB (Multi Harmonic Buncher), as the present design may restrict us in achieving a bunch width of less than 1.5 ns which is the design requirement of the RFQ.

2.2 Free electron laser based THz facility

B. K. Sahu¹, P. Patra¹, J. Karmakar¹, B. Karmakar¹, M. Aggarwal¹, A. Sharma¹, S. R. Abhilash¹, A. Kothari¹, T. Vurughe¹, S. K. Saini¹, G. K. Chaudhari¹, P. Barua¹, Chandrapal¹, R. Kumar¹, S. K. Suman¹, P. K. Verma¹, S. Venkataraman¹, P. Singh¹, A. Kumar¹, R. N. Dutt¹, V. V. V. Satyanarayana¹, K. Singh¹, R. Shanti¹, D. K. Munda¹, Y. Mathur¹, P. K. Mukhopadhyay⁵, V. Naik², T. Rao³, A. Aryshev⁴, S. Ghosh¹, R. K. Bhandari¹ and A. C. Pandey¹

¹Inter University Accelerator Centre, Aruna Asaf Ali Marg, New Delhi, India

²Variable Energy Cyclotron Center, Kolkata, India

³Brookhaven National Laboratory, USA

⁴High Energy Accelerator Research Organization, KEK, Tsukuba, Japan

⁵Raja Ramanna Centre for Advanced Technology, Indore, M.P., India

The compact pre-bunched Free Electron Laser facility named as Delhi Light Source (DLS), was commissioned and presently producing electron beam for conducting experiments in Materials Science, Biology and Atomic physics. Last year, after final installation of the high-power RF source with Circulator, RF Conditioning of the RF gun could be performed up to 5 MW of RF power and production of electron beam up to 4.5 MeV was demonstrated and measured using dipole magnet I and Integrated Current Transformer (ICT). This year, the beam line from dipole magnet I had been extended up to the beam dump installed after dipole magnet II. Now the complete beam line is equipped with both the Dipole magnets using 60 degree achromatic bends, Beam Position monitors, Beam viewers, ICTs, vacuum pumps etc. Two different experimental chambers were installed to perform experiments with the electron beam. The THz extraction chamber equipped with Ti-foil to reflect THz radiation at 45° angle was also installed post undulator section and efforts are presently being dedicated to detect THz radiation produced by the undulator using a pyroelectric detector. The development of fiber-based laser system for this facility in collaboration with KEK

Japan was completed and the system had successfully produced electron beam at LUCX facility of KEK. The laser system had been transported to IUAC and was installed at IUAC. It is expected that in the next few months, the electron beam with the beam width of a few hundred of femto-seconds will be produced from the electron gun and the same will be injected into the compact undulator for production of coherent THz radiation.

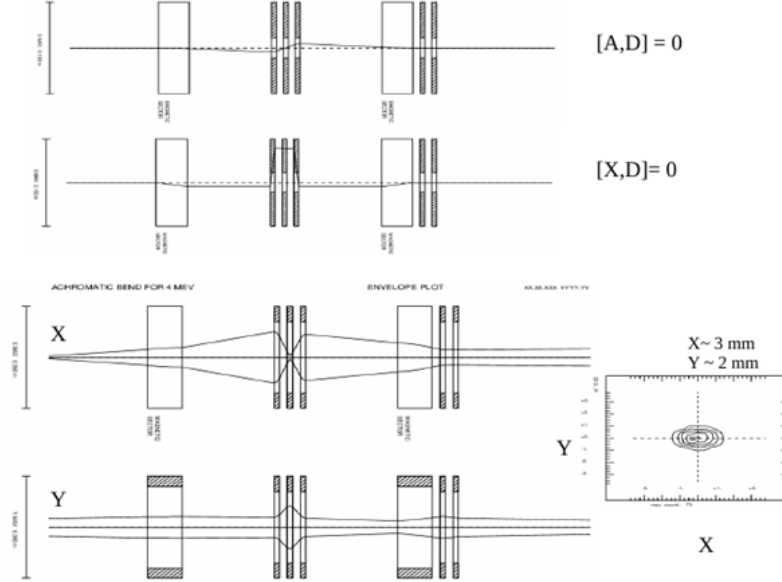


Figure 2.18: : The upper two plots show $[A,D]$ and $[X,D]$ are made zero as required for an achromat. The lower plots show the X and Y envelope variation through the achromat and the beam transverse size 1 m after the second bend.

2.2.1 Status of various subsystems of DLS

The progress of the various activities related to the setting up of the compact FEL are listed in the following sub-sections:

2.2.1.1 Commissioning status of the electron beam line

During the last academic year, the Undulator Magnet along with its narrow vacuum chamber had been precisely aligned and the beam energy was measured by using the first dipole magnet installed at the first achromatic bend. In this academic year another dipole magnet along with magnetic quadrupole triplet and steering magnets were installed to complete the achromatic bending section of the electron beam line. The sixty degree (60°) bending section of the second dipole magnet was aligned with the experimental chamber along with the quadrupole doublets and steering magnet for the delivery of electron beam to the experimental chambers to be dedicated for electron beam related experiments. The beam line between the achromatic bends is ~ 2 m in length and the position of the quadrupole triplet between the bends, to act as an achromat, was initially designed with separation between the quadrupoles as 150 mm. During installation of the beam line components and diagnostics elements such as the BPM, diagnostic chamber, valves, ICT, it was found that 150 mm separation between the quadrupoles of the triplet was not feasible. The optimum separation between the three quadrupole magnets of the triplet is limited to be 70 mm. In order to check the achromatic bending section of the beam line, fresh simulations were carried out with the triplet having modified separation of 70 mm. The simulations were done using GICOSY concluded that the installed quadrupole triplet with 70 mm separation can still be used to meet the achromatic condition along with a focussed beam. The results of the simulation for 4 MeV beam with beam input taken from the output of the beam through the undulator is shown in Fig. 2.18. The zero-degree line of the first dipole magnet (the electron beam will be going straight along the zero-degree beam line when this magnet will be kept off) was also aligned with an additional experimental chamber for atomic physics experiments. The BPM along with

2. ACCELERATOR AUGMENTATION

ICT were also installed in this beam line for tuning of the beam to the experimental chamber. The view of the installed beam line post undulator section along with design drawings of the entire beam line is shown in Fig. 2.19.

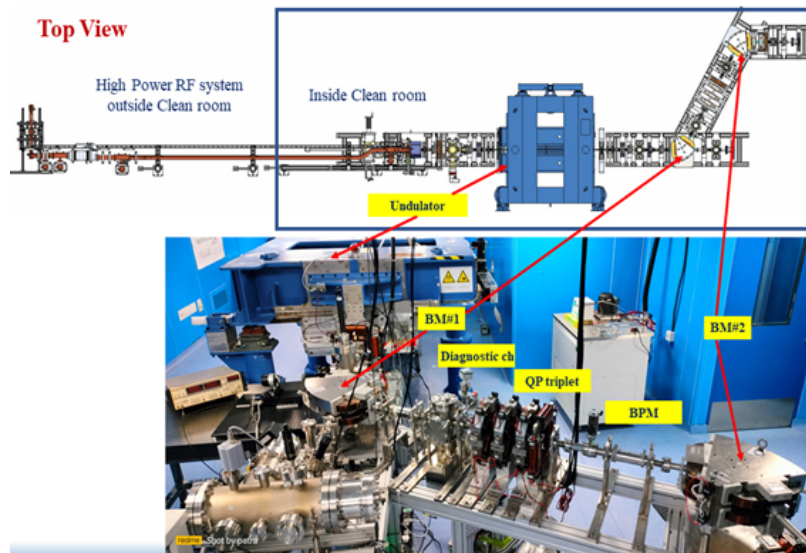


Figure 2.19: The complete beam line for post Undulator section along with the second Dipole magnet and the quadrupole triplet

2.2.2 Status of RF conditioning of photocathode gun

During the last Academic year, after installation of the SF6 based Circulator, rigorous RF conditioning of the RF photo cathode gun was initiated in 24×7 mode and maximum RF field gradient of 65 MV/m (at 4 MW of RF Power) was generated inside the photo cathode gun. However, due to operational constraints and excessive radiation levels, the machine could only be operated at night and an operator was assigned to monitor the RF Conditioning throughout the night. At higher field gradients, due to excessive electron discharge or arcs at the RF junctions, several anomalies occurred that caused high reflected power, which in turn affected the cavity or waveguide vacuum conditions and caused the system to trip. The trip happened when the high-power RF was stopped reaching the cavity due to the failure of one or many of the interlocks imposed on the high-power RF system. It was realized that if the ion-pump current is continuously monitored by the operator and the input drive power was changed accordingly, it is possible to prevent the system from tripping and the effective conditioning hours could be increased. It was, however, impractical to have such an arrangement due to human limitations as it was extremely difficult for the operator to prevent the system from tripping. In order to avoid such incidents and to reduce the frequency of the trips of the RF system, a machine learning algorithm was developed that could predict a sustainable and stable vacuum / pressure levels at different RF power levels and if the vacuum level ever went out of control, then it would reduce or control the power level automatically to prevent the system from tripping. The most important parameters of the RF cavity conditioning are the vacuum of the RF Gun i.e. ion pump control current of IPC07 (the last Ion Pump in the Wave Guide section connected to the Cavity) and the set power level. The entire control algorithm did operate only by changing the set power level with the fluctuations of the IPC07 current. The RF forward power was also considered as an important variable as its value falling to zero indicates a trip, and the designed algorithm wanted to prevent the same. The implemented model was based on the use of an unsupervised learning model called K-means Clustering, a supervised linear regressor and a Decision tree classifier. Currently this program is being deployed in the control scheme for uninterrupted RF conditioning of the photocathode Gun and the system is being conditioned for 10 MW of RF Forward power. The Energy of the produced electron beam was measured to be 6 MeV at 9 MW of RF Power. An EPICS GUI is also developed for monitoring and recording of various parameters during RF Cavity conditioning.

Table 2.3: Experiments using electron beam facility of FEL

User and Affiliation	Experiments	Energy of the electron beam	Total beam time (hours)
Dr. C.P. Safvan Atomic Physics IUAC	Measuring ionization cross section with high energetic electron beam	2 MeV	40
Dr. Praveen Kumar JNU student	Effect of e-beam on activated carbon to enhance its removal property of heavy metal toxic elements in water	2 MeV	12
Dr. Hemen Mendhi, St. Edmund's College Shillong	Irradiation on Bakelite sample (for Nuclear detector) delivering accumulated dose by e-beam	4 MeV, 5 MeV	8
Ms. Sadiya Samar Chaudhary Charan Singh University Meerut	Low Energy Electron Beam affecting physiological and biochemical attributes of Garden Pea Plant in association with ZnO nanoparticles, Total 60 samples were irradiated	5 MeV	24

2.2.3 Production of high energy electron beam for user experiments

During the last academic year, a nanosecond UV laser having wavelength 266 nm was made to incident on the cathode to produce electrons from the copper photocathode and electron beam energy values at different accelerating fields of the electron gun along with the charges were measured. This academic year, the possibility of using the produced electron beam for various user experiments was explored. A user workshop was also arranged on December 27, 2023 where a number of proposals were suggested for electron beam related experiments. However, among them, 7 feasible experiments using the electron beam were presented in the workshop for conducting experiments. Four numbers of experiments using the electron beam facility of FEL, as listed in Table 2.3, have been conducted in this academic year.

2.2.4 Status of the photocathode deposition system

At present, the production of electron beam is being continued by striking the laser beam on the Cu photocathode. In order to improve the quality of the electron beam in terms of bunch width, emittance, energy spread, etc., semiconductor photocathode (Cs_2Te) deposition system had been installed in last academic year. After installation of photocathode deposition system along with other accessories like vacuum elements, magnetic manipulators, source chambers etc., the evacuation was done and a leak rate of 5×10^{-12} mbar had been achieved. Installation of the source assembly and the temperature calibration of cathode substrate was completed. The positioning of the Quartz Crystal Monitor (QCM) with respect to the substrate was optimized by measuring $\sim 1/5$ th of film thickness measured by QCM compared to the deposition thickness on the substrate. A UV LED system was installed just outside the deposition chamber and the laser beam was aligned so that it would hit the substrate kept inside the deposition chamber to measure the quantum efficiency of the photo cathode during deposition. It is expected that the first successful deposition of Cs_2Te thin film on Molybdenum substrate will be demonstrated in next 6 months.

2.2.5 Status of the development of the fiber laser system

The laser system is one of the most crucial subsystem of the Delhi Light Source (DLS) facility for the production of THz radiation. A state-of-the-art Fiber Laser system to produce ultra-short laser pulses with energy $\sim 1.5 \mu\text{J}$ at UV (255 nm) with a pulse width of < 500 fs was developed as a collaborative project between IUAC and High Energy Accelerator Research Organization (KEK), Japan. During this academic year, the development of the laser system was successfully completed and the production of electron beam from KEK's electron gun was demonstrated by using the Fiber Laser system of IUAC. Fig. 2.20 shows the complete fiber laser system including the Oscillator, Pulse Picker, Stretcher, Pre-pre amplifier, Pre-amplifier,

2. ACCELERATOR AUGMENTATION

Amplifier-I, Amplifier-II, Compressor and the system for Fourth Harmonic Generation (FHG). Fig. 2.20 also shows some of the measured parameters.

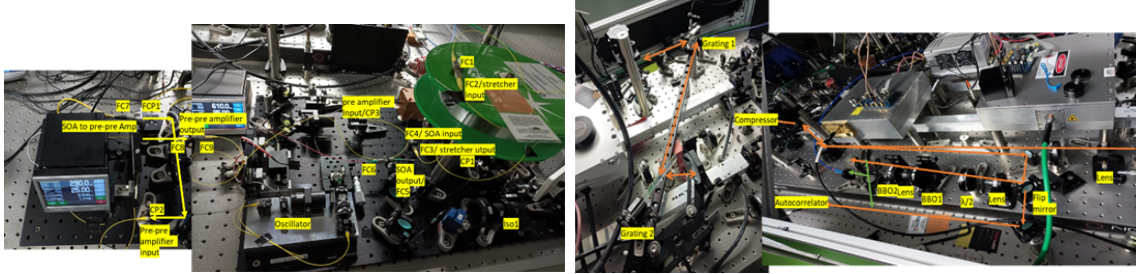


Figure 2.20: (Top): oscillator, pulse picker (SOA), fiber stretcher, pre-pre-amplifier and pre-amplifier (Bottom): Main amplifiers, compressor grating and harmonic generation line.

The major modifications and the noteworthy achievements towards the success of the development of the laser device are given below:

- Tuning and optimization of the Oscillator output for stable 130 MHz mode-locked ultrashort pulses (~ 1 ps) with sufficient bandwidth (~ 25 nm).
- Enhancement of the width of the stretched laser pulse up to ~ 360 ps by installing 500 m fiber pool to maximize the gain through chirped pulse amplification technique.
- Optimization of the Semiconductor Optical Amplifier (SOA) for selection of the desired number of laser pulses in the multi-micro pulse formation inside the 4 microsecond window at 10 Hz burst rate.
- Adaptation of pulsed mode amplification through pre-amplifier and main amplifiers to achieve maximum of ~ 15 mJ burst energy at IR with the designed pulse structure.
- Successful compression of the amplified pulses to less than 500 fs with new compressor grating.
- Successful demonstration of Fourth Harmonic Generation by converting IR to green and then green to UV.

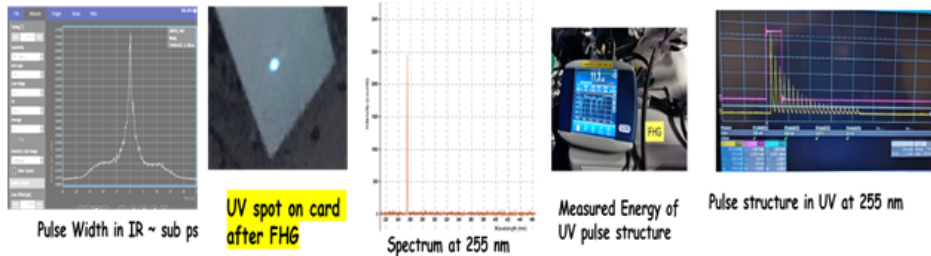


Figure 2.21: Fiber Laser system along with the measured parameters.

The laser system was transported to Delhi in March 2024 and is being installed inside the laser hut of the DLS facility along with all the sub-systems.

In conclusion, the commissioning of the compact Free Electron Laser at IUAC for the production of electron beam was accomplished and production of THz beam is in its final phase. The RF conditioning of the electron gun was performed up to 10 MW of peak RF power for the desired $4 \mu\text{s}$ duration. The electron beam up to 6 MeV was measured and the beam was delivered for conducting experiments in Atomic Physics, Biology and Materials Science. High power RF conditioning is being continued beyond RF power of 10 MW for $4 \mu\text{s}$ pulse duration for achieving the maximum electron beam energy of 8 MeV. With the installation of the new fiber laser system, the quality of the electron beam should improve and after injecting the better quality electron beam into the compact Undulator, the production of THz radiation is expected to be demonstrated soon.